Electron-phonon coupling of *G* mode and assignment of a combination mode in carbon nanotubes

Y. Yin (尹 彦),[1,2,*] A. G. Walsh,[2] A. N. Vamivakas,[3] S. B. Cronin,[4] D. E. Prober,[5] and B. B Goldberg[2,3,†]

[1]*Key Laboratory of Optical Physics, Institute of Physics, Chinese Academy of Sciences, Beijing 100190, P. R. China*
[2]*Department of Physics, Boston University, Boston, Massachusetts 02215, USA*
[3]*Department of Electrical and Computer Engineering, Boston University, Boston, Massachusetts 02215, USA*
[4]*Department of Electrical Engineering, University of Southern California, Los Angeles, California 90098, USA*
[5]*Department of Applied Physics, Yale University, New Haven, Connecticut 06520-8284, USA*

We measure the electron-phonon (e-ph) coupling matrix elements of the *G* band in semiconducting carbon nanotubes (CNTs) in comparison to the radial breathing mode (RBM). The experimental result for the G^+ mode [Γ-point longitudinal optical (LO) phonon] at the E_{22} transition suggests an e-ph coupling strength of approximately 30 meV or 12.5 eV/Å, which is within the expected range of 23 meV to 83 meV for a 1-nm-diameter CNT. This coupling (as the square of the matrix elements) for the G^+ mode is an order of magnitude higher than that of the RBM and other measured phonon modes. In addition we assign a Raman feature observed around 1700 cm^{-1} to be the combination mode of a low energy ($\sim$400 cm^{-1}) and a high energy ($\sim$1300 cm^{-1}) zone-boundary phonon. Both the phonon energies and phonon dispersions of those modes support the assignment.

PACS number(s): 78.67.Ch, 63.22.−m, 73.63.Fg, 78.30.−j

Electron-phonon (e-ph) coupling is a fundamental physical process that controls e-ph scatterings in the transport properties of electronic devices[1] and mediates the electron-electron interaction[2,3] as well as most light-matter interactions (e.g., Raman, photoluminescence). In the field of carbon nanotubes (CNTs) researchers commonly maintain the source-drain bias voltage on a CNT below a threshold of approximately 100 meV to reduce the e-ph scattering in the device. This is based on an understanding that the longitudinal optical (LO) phonon, the high-energy phonon mode, is the primary source of e-ph scattering. Such an understanding comes from both transport measurements[4,5] and theoretical calculations.[6] In fact researchers reported the selective excitation of LO phonon with an injecting electron current.[7] Therefore, experimental studies of the e-ph coupling from LO phonon in CNTs are highly important and hold good scientific values in the field. The optical measurements of the e-ph coupling for the *G* mode in CNTs have been reported a couple of times. One of them uses the broadening of the Raman-line widths in the metallic CNTs to find out the e-ph coupling of the *G* modes.[8] Another method measures the oscillation of the coherent phonon by the femtosecond pump-probe technique.[9] The latter report converts the time-domain oscillations to energy-domain Raman features, uses the resulting broad "Raman line widths" to calculate e-ph coupling, and gives large e-ph coupling values.

In an earlier report we demonstrated that the e-ph coupling in CNTs can be quantitatively determined by correlating the first- and second-order intensities of the radial breathing mode (RBM).[10] We used resonance Raman scattering to optically measure the e-ph coupling strengths of RBM in the CNTs.[10,11] Our method enables us to probe different phonon modes simultaneously and without damaging the nanotubes. In this report we measure different Raman modes, including the RBM and G^+ modes, from two CNTs (9,4) and (9,7). The resonant Raman scattering excitation (RRSE) profiles of those modes are extracted from the Raman spectra and are analyzed to study

their relative e-ph coupling strengths. Having established a quantitative value for RBM mode as a reference point, we can obtain the absolute values of other modes. We present the e-ph coupling values for the *G* band and its comparison to RBM phonons. Our experimental results are consistent with the general understanding that the LO phonon is the dominant e-ph coupling (or scattering) source under high-bias conditions and are quantitatively linked to the findings from transport measurements of CNTs and graphene.[1,12] In addition another high-energy Raman feature observed around 1700 cm^{-1}, referred to as the *M* band, is also measured and discussed. An earlier report proposes that this *M* band originates from the overtone of the out-of-plane transverse optical (oTO) phonon mode at 867 cm^{-1} in graphite,[13] rather than the combination of the RBM and *G* band, as was originally thought.[14] However, our experiment result suggests that the so-called *M* band is a combination mode of two zone-boundary phonons. One is a high energy (about 1300 cm^{-1}) zone-boundary phonon; the other is a low energy (about 400 cm^{-1}) zone-boundary phonon likely corresponding to a longitudinal acoustic (LA) phonon in graphite after zone folding in CNTs.[15,16] This assignment is based not only on the *M* mode's connection in energy with other phonon modes of the same CNT but also on the connection of phonon dispersions of those three modes.

The CNT samples in this study are grown by chemical vapor deposition (CVD) method over prefabricated trenches on quartz subtrates.[17,18] The trenches are about 1–1.5-μm wide. The CNTs are believed to be in small bundles based on their largely red-shifted E_{22} electronic-transition energies and also their branched-looking features observed in scanning electron microscopy (SEM) images.[18] However, the CNTs in this study are individually measured on different samples, only one CNT is in resonance with the excitation laser and only its Raman features are observed. The tunable Raman microscope system is modified from a commercial single excitation Renishaw Raman microscope. A Ti-sapphire tunable Laser (720–830 nm)
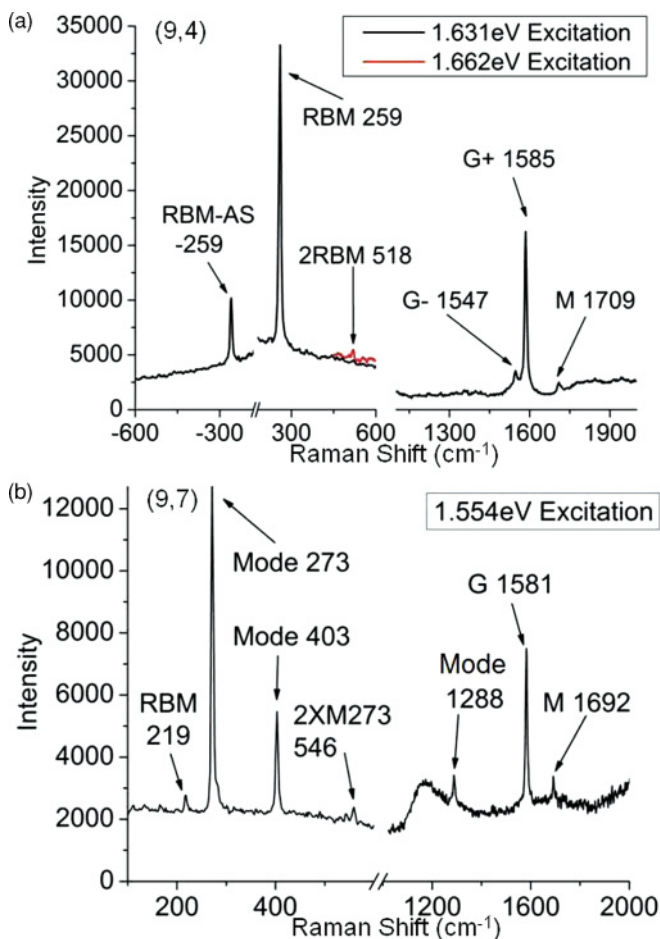
FIG. 1. (Color online) Raman spectra of the measured CNTs. (a) Raman spectrum of CNT (9,4) at 1.631-eV excitation and 1.662-eV excitation with a better signal for the 2RBM mode. (b) Raman spectrum of CNT (9,7) at 1.554-eV excitation. Raman intensities are in arbitrary units.

is used as the excitation source with an illumination power lower than 2 mW focused onto the sample by a $100\times$ objective lens (NA 0.90). The Raman features from one CNT are collected simultaneously for each excitation wavelength.

Figure 1(a) and 1(b) show the Raman spectra taken from a (9,4) CNT at an excitation energy of 1.631 eV and 1.662 eV and a (9,7) CNT taken at 1.554 eV. In Fig. 1(a) the spectrum for the (9,4) nanotube taken at 1.662 eV is a partially resonant Raman spectrum for the 2RBM (518 cm^{-1}), the overtone of the RBM mode. The Raman spectrum of this CNT taken at 1.631 eV shows not only the RBM and 2RBM (very weak here), but also the anti-Stokes RBM (-259 cm^{-1}), G^- (1547 cm^{-1}), G^+ (1585 cm^{-1}),[19] and M mode (1709 cm^{-1}). Figure 1(b) shows the Raman spectrum of (9,7) CNT taken with 1.554-eV excitation and exhibits the RBM (219 cm^{-1}), the mode 273, the mode 403 (possibly a zone boundary-phonon mode originating from LA mode after zone folding),[15] the overtone of the mode 273 (546 cm^{-1}), the mode 1288, G^+ mode (1581 cm^{-1}), and M mode (1692 cm^{-1}). The assigned (9,7) CNT might be a CNT with defects, especially if the mode 1288 is the D mode. At the same time (9,7) CNT's simple, sharp, and unshifted (smaller than 10 cm^{-1}) G mode has the same resonance behavior with those of other modes.

This supports that the observed CNT is an individual structure. Tunable Raman mappings are performed on both CNTs. The intensities of each Raman mode are determined from their integrated areas. The RRSE profiles are, thus, obtained by plotting their intensities as a function of the excitation-photon energy. Figure 2(a)–2(f) show the RRSE profiles (the hollow circles) for anti-Stokes RBM, RBM, G^-, G^+, 2RBM, and M modes of the (9,4) CNT in Fig. 1(a). The similar process for the (9,7) CNT is also performed as well. We use standard perturbation theory[20] to calculate and fit the RRSE profiles of these Raman modes and thus extract the e-ph coupling matrix elements for the corresponding phonon modes.

The resonant Raman cross section for first-order, one-phonon scattering is given by[10,20,21]

$$\frac{d_1\sigma'(E_L,E_{ph},\theta)}{d\Omega} = A\frac{(E_L - E_{ph})^2}{E_{ph}^2 E_L^2}\left| \frac{1}{\sqrt{E_L - E_{ii} - i\eta}} \right.$$
$$\left. - \frac{1}{\sqrt{E_L - E_{ph} - E_{ii} - i\eta}} \right|^2, \quad (1)$$

where we define $A = CN_{ph}|M_{e-ph}|^2$. C is a tube-dependent constant which includes photon-energy independent parts of the optical-matrix elements. In our calculation only one electron and hole band with a transition energy E_{ii} are considered; E_L is the excitation photon energy; E_{ph} is the phonon energy; and η is the broadening factor in units of energy. M_{e-ph} is the e-ph transition-matrix element, denoted for a particular phonon branch, at a particular phonon wave vector (the zone center Γ point phonon here) and under a particular electron transition (E_{22} in this report). The overall e-ph coupling strength in a one-phonon resonant Raman scattering process is $N_{ph}|M_{e-ph}|^2$, where $N_{ph} = (n_{ph} + 1)$ for Stokes scattering and $N_{ph} = n_{ph}$ for anti-Stokes scattering; $n_{ph} = 1/(e^{|E_{ph}|/kT} - 1)$ is the phonon number. Temperature T is 300 K for the calculation and is verified by the RBM Stokes and anti-Stokes intensity ratio. For a same CNT at the same resonant energy E_{ii}, C is a constant value; therefore, the parameter A/N_{ph} is proportional to the $|M_{e-ph}|^2$ for the different phonon modes. The relative e-ph coupling strength of those modes can be extracted by this method.

In addition the absolute value of the e-ph coupling from one mode can be obtained by correlating its first and second-order resonant Raman excitation profiles.[10] A Γ-point phonon's contribution to the two-phonon Raman scattering cross section can be described as[22]

$$\frac{d_1\sigma'(E_L,E_{ph},\theta)}{d\Omega} = A'\frac{(E_L - 2E_{ph})^2}{E_L^2}$$
$$\times \left| \frac{(p_1+p_2+p_3)}{(p_1+p_3)(p_1+p_2)(p_3+p_2)} \cdot \frac{1}{p_1 p_2 p_3} \right|^2, \quad (2)$$

where we define $p_j = \sqrt{E_L - E_{ii} - (j-1)E_{ph} - i\eta}$, $j = 1,2,3$, and $A' = CN_{ph}^2|M_{e-ph}|^4 w_\Gamma$. The constant C is the same constant in the one-phonon scattering equation. Theoretical calculation shows that w_Γ, the phonon density of states weight factor at Γ point, is approximately 1 for chiral single-walled nanotubes (SWNTs).[10,23] Then we can use $|M_{e-ph}|^2 = A'/(w_\Gamma AN_{ph})$ to obtain the absolute values of the e-ph coupling matrix elements.[10] The value from this mode
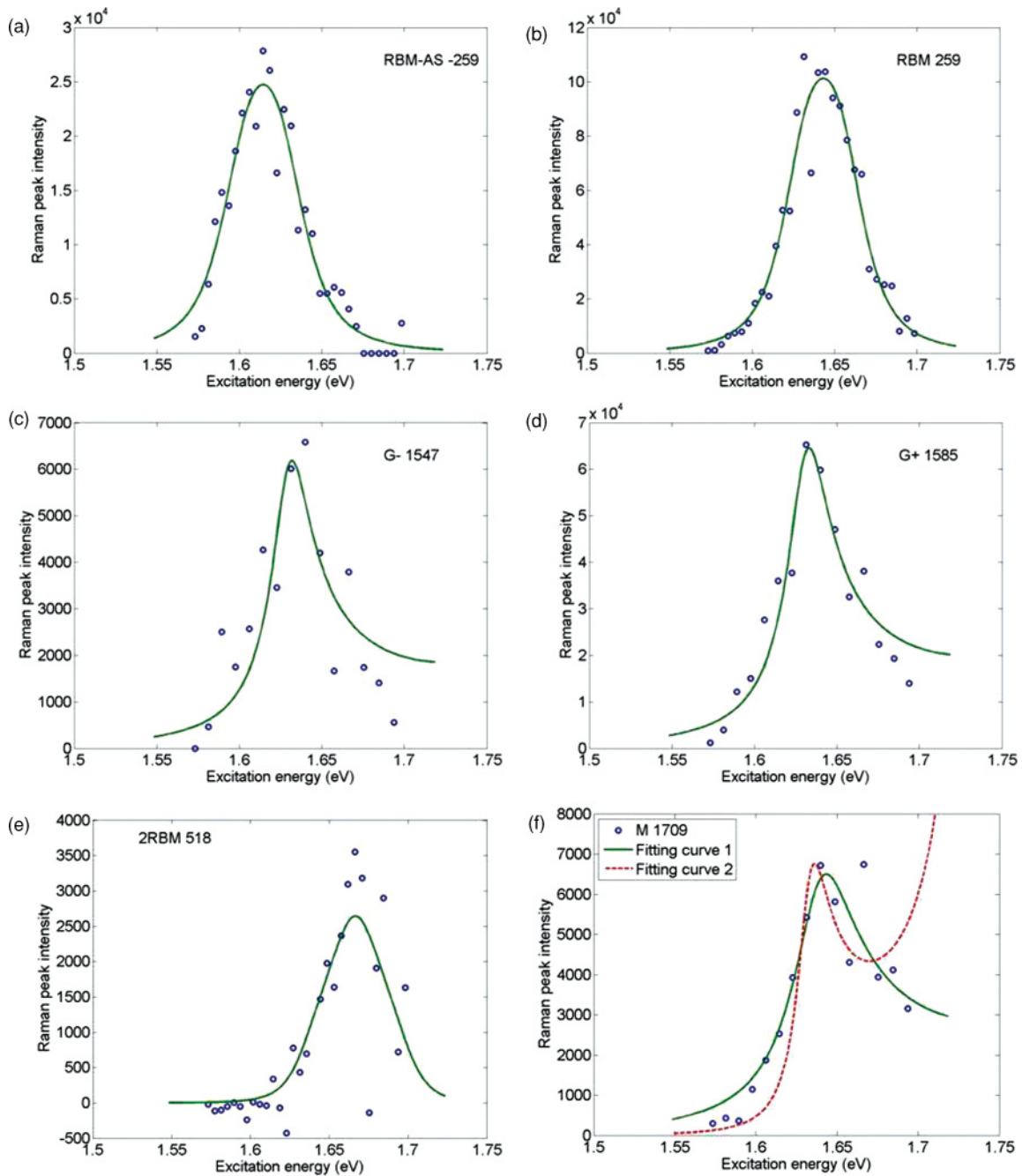
FIG. 2. (Color online) Raman-excitation profiles of the (a) anti-Stokes RBM, (b) Stokes RBM, (c) G^-, (d) G^+, (e) 2RBM, and (f) M modes of the CNT (9,4). The hollow circles are experiment data, and the curves are fitting results. The green solid curve in subfigure (f) is a fitting with Eq. (1) for a combination of two zone-boundary phonons, and the red dash curve is a fitting with Eq. (2) for an over tone mode. Raman intensities are in arbitrary units.

can be used as a reference point for other modes; therefore, the absolute values of all other phonon modes can be obtained by resonant Raman studies as well.

Equation (1) is used to fit the RRSE profiles of one-phonon Raman modes, namely the anti-Stokes RBM, RBM, G^-, G^+ for the (9,4) CNT and the RBM, M273, M403, M1288 and G^+ for the (9,7) CNT. Equations (1) and (2) correspond to optical phonon scatterings at the Γ point ($q = 0$). In principle both equations should not be used for calculating the M403 (LA) and M1288 mode profiles, however, the resonance locations

(incoming resonance and outgoing resonance) should be accurate from fittings with those equations. Therefore, we still fit the incoming resonance data of M1288 and M403 (LA) with Eq. (1) to obtain the E_{ii} and help demonstrate that all modes come from the same CNT. The fitting curves for the anti-Stokes RBM, RBM, G^-, G^+, 2RBM of the (9,4) CNT are plotted in Fig. 2(a)–2(e) as green solid lines for demonstration. The values of A, η, and E_{ii} (E_{22} here) for different modes are obtained from the fitting of the one-phonon Raman modes and are listed in Table I for both CNTs (9,4) and (9,7). Equation (2)

TABLE I. Measurement results, fittings, and the e-ph coupling matrix elements for different Raman modes of CNT (9,4) and CNT (9,7) at the E_{22} transition. The last column lists the e-ph coupling matrix elements from theoretically calculations.[24] The theoretical values are retrieved from the reported paper after applying $|M_{e-ph}| = |g|/\sqrt{N_u}$.

CNT	Mode type	Mode	Shift (cm^{-1})	A or A'	η (meV)	E_{22} (eV)	$\overline{E_{22}}$ (eV)	$|M_{e-ph}|^2$ $(\times 10 \ meV^2)$	$|M_{e-ph}|$ (meV)	$|D|$ (eV/Å)	$|M_{e-ph}|$ theory (meV)
(9,4)	One-phonon	RBM-AS	-259	1.7 ± 0.6	22 ± 4	1.631 ± 0.002	1.630 ± 0.002	5 ± 2	7 ± 1	1.1 ± 0.2	9.7
		RBM	259	6 ± 2	19 ± 4	1.627 ± 0.002		5 ± 2	7 ± 1	1.1 ± 0.2	9.7
		G^-	1547	5 ± 2	12 ± 6	1.629 ± 0.005		6 ± 2	7 ± 1	2.7 ± 0.4	6.1
		G^+	1585	56 ± 11	12 ± 3	1.630 ± 0.003		65 ± 26	26 ± 5	10 ± 2	26.5
	Two-phonon	2RBM	518	$(4 \pm 1) \times 10^{-4}$	19	1.633 ± 0.009		5 ± 2	7 ± 1	1.1 ± 0.2	9.7
(9,7)	One-phonon	RBM	219	0.3 ± 0.4	38 ± 19	1.554 ± 0.009	1.548 ± 0.004	0.9 ± 0.6	3 ± 1	0.5 ± 0.2	3.8
		M273	273	4 ± 2	28 ± 8	1.545 ± 0.004		10 ± 8	11 ± 4	2.1 ± 0.8	N/A
		M403	403	0.7 ± 0.5	18 ± 10	1.548 ± 0.004		N/A	N/A	N/A	N/A
		M1288	1288	1.5 ± 0.4	11 ± 4	1.552 ± 0.003		N/A	N/A	N/A	N/A
		G+	1581	24 ± 7	18 ± 6	1.549 ± 0.005		100 ± 70	32 ± 11	15 ± 5	21.2
	Two-phonon	2M273	546	$(6 \pm 2) \times 10^{-4}$	28	1.54 ± 0.01		10 ± 8	11 ± 4	2.1 ± 0.8	N/A

is used to fit the RRSE profiles of the two-phonon Raman modes for these two CNTs, 2RBM of (9,4) in Fig. 2(e), and 2M273 of (9,7). Their fitting results for A' (sharing a same column with A in one-phonon modes), η, and E_{22} are listed in Table I as well. The $\overline{E_{22}}$ of both CNTs are the averages of the E_{22} values from their individual modes and are followed by their standard deviations. The E_{22} value of each mode of both CNTs is within its error range compared to $\overline{E_{22}}$. This supports that different phonon modes from a CNT have a same E_{22} resonance energy. By correlating the first-order and their overtone Raman features, we can obtain the absolute values of the e-ph coupling matrix elements, $|M_{e-ph}|^2$, for the RBM of (9,4) and M273 of (9,7).[10] Those coupling values are used as the reference points for corresponding CNTs to calculate the e-ph coupling matrix elements of other Raman modes by comparing relative strengths, which are proportional to A/N_{ph}. All of the resulting $|M_{e-ph}|^2$ and $|M_{e-ph}|$ values are listed in Table I. The relative e-ph coupling values for the anti-Stokes RBM (RBM-AS) and the Stokes RBM (RBM) of (9,4) are obtained independently from their RRSE profiles. As expected, they show identical results. In the literature the e-ph coupling strength sometimes is also referred to as matrix elements D in units of eV/Å. This D represents the overall deformation potential of e-ph coupling, thus it is in the units of a deformation potential and can be linked to our discussion with $M_{e-ph} = -x \cdot D$, with x as the amplitude of a particular phonon mode. $x = \sqrt{\hbar/(N_u m_C \omega_{ph})}$, where $\hbar$ is the reduced Plank constant, N_u is the number of the graphite unit cells in the CNT unit cell, m_C is the mass of the carbon atom, and ω_{ph} is the phonon-angular frequency.[24] The corresponding deformation potentials $|D|$ are calculated from the measured $|M_{e-ph}|$ using the above formula and are listed in Table I. The theoretical results for $|M_{e-ph}|$ are extracted from Jiang *et al.*'s published report[24] and are listed in the last column of Table I for comparison. Jiang *et al.* use an extended tight-binding model and give similar e-ph coupling values as those reported in another paper using numerical *ab initio* calculation.[25] The

theoretical values are converted with $|M_{e-ph}| = |g|/\sqrt{N_u}$, where $|g|$ is the non-normalized e-ph coupling matrix elements calculated in Jiang *et al.*'s paper.[24]

For the values of the e-ph coupling matrix elements, our experiment presents 26 ± 5 meV and 32 ± 11 meV for the G^+ mode in (9,4) and (9,7). The G^- mode (zone-boundary in-plane transversal optical, iTO, phonon) has a value of 7 meV in (9,4). The RBM modes have values of approximately 7 meV and 3 meV for (9,4) and (9,7), correspondingly. Most of the measured $|M_{e-ph}|$ are in good agreement with existing theoretical values, although the value for the RBM of (9,4) is somewhat smaller than the theoretical one. This implies that the tight-binding model does produce good values for semiconducting CNTs, and the deformation potential is indeed the physical origin for e-ph coupling in semiconducting CNTs. The deformation potentials $|D|$ for the G^+ mode (LO phonon at Γ point) are 10 ± 2 eV/Å and 15 ± 5 eV/Å for (9,4) and (9,7). The numbers are very close to the value, 12.8 eV/Å, used in CNT-transport measurements.[1] This association is important and demonstrates that the e-ph coupling strength measured from this optical method can be directly used in the analysis of transport measurements. In addition our values are in close match with the value 12.6 eV/Å, measured from single-layer graphene by a combined transport and optical method.[12] Another earlier report studied G-band Raman-line broadenings in metallic CNTs and gave a |D| value of 6 eV/Å.[8] This value is about half of previous numbers but is within the same order of magnitude.

Now we compare the e-ph coupling strengths of different phonon modes in the two CNTs. First those e-ph coupling values are not the direct reflections of their Raman cross section. For example, the G^+ mode intensity is only about half of the Stokes RBM intensity for (9,4) in Fig. 1(a), whereas the M_{e-ph} for G^+ mode is much larger than that of the RBM mode. This is because the resonance term in (1) is proportional to the $1/E_{ph}^2$ when $E_L \approx E_{ii}$. It means that $|M_{e-ph}|$ values for high-frequency modes are normally much

larger than they appear to be in a resonant Raman spectrum. In Table I the G^+ mode has the exceptionally strongest $|M_{e-ph}|^2$ values as compared to other modes. $|M_{e-ph}|^2$ is the physically measureable value for e-ph coupling strength. Its value for G^+ is about 10 times larger than the second strongest mode in both CNTs. In semiconducting CNTs the physical origin of e-ph coupling for all phonon modes is same, the deformation potential. The strong coupling for the G^+ mode is attributable to its LO-phonon nature. Under the LO-phonon vibration (the G^+ mode), the two sublattices of graphene move coherently in opposite directions (or phase) and along the nearest carbon-carbon bond direction. For the same amount of vibrational amplitude, a much larger changing of the electron-gas overlapping among the nearest atoms occurs for the LO mode than those of other modes. (For example, the RBM mode is an oTO vibration perpendicular to the C bonds.) Thus, a much stronger e-ph coupling is expected for LO phonon. The fact that LO phonons dominate the e-ph coupling is consistent with reported transport experiments under high fields.[1,4,7] We need to take note that the measured RRSE profile intensities for the M1288 and M403 modes in our method do not represent their intrinsic e-ph coupling strengths. The M1288 and M403 modes are second-order one-phonon scattering[15] and are defect-dependent Raman modes. Their Raman intensities rely on a finite defect density. In addition Eq. (1) is for Γ-point phonon and does not reflect the *q*-dependent nature of the second-order one-phonon scattering.[20,22] The *D* band (K-point LO phonon) is expected to have a stronger e-ph coupling than G^+ mode. The K-point LO phonon is more important than Γ-point LO phonon for electron transport at high field.[1,6]

In the earlier report we detailed the RBM e-ph coupling as a function of diameter and chirality and showed that it follows a Goupalov analytic solution.[10] Here we discuss the diameter and chirality dependence of e-ph coupling for Γ-point LO phonons. Jiang *et al.* used the standard tight binding and extended tight binding model to calculate the Γ-point LO phonon e-ph coupling in semiconducting CNTs.[24,26] Both papers present the e-ph coupling as |g| in non-normalized units of $\sqrt{N_u}$. N_u is the number of the graphite unit cells in the CNT unit cell. In such a unit the e-ph coupling |g| of Γ-point LO phonon for diameter and chirality dependency is mostly flat in the standard tight-binding model.[26] It has a small (smaller than 25% in dynamic range) variation in the extended tight-binding model and can be approximated as a constant, about 0.42 eV for E_{22} transition.[24] Converted to normalized units, $|M_{e-ph}| = |g|/\sqrt{N_u} = (a_0/\sqrt{2}\pi) \cdot |g| \cdot \sqrt{\gcd(2n+m, 2m+n)}/d$, where a_0 is the graphite unit length 2.461 Å, *d* is the tube diameter, gcd( ) is the greatest common divisor function, and *n* and *m* are the CNT indexes. In general, a larger diameter CNT tends to have a smaller $|M_{e-ph}|$ for Γ-point LO phonon. For CNTs with the same diameters at E_{22} transition, a zig-zag $(n, 0)$ CNT gives the largest $|M_{e-ph}| = (\sqrt{a_0/2}\pi) \cdot |g|/\sqrt{d} = (0.26$ eV· Å $^{1/2})/\sqrt{d}$. CNTs (n,m), semiconducting mod(n-m,3) $\neq 0$, with no common factor in *n,m* other than 1, give the minimum $|M_{e-ph}| = (a_0/\sqrt{2}\pi) \cdot |g|/d = (0.23$ eV· Å $)/d$. $|M_{e-ph}|$ for the rest of the CNTs are distributed between those two limits, depending on their (n,m). For 1-nm-diameter CNTs (mostly studied by optical methods), these low and high limits are

23 meV and 83 meV. They are 12 meV and 58 meV for CNTs with 2-nm-diameter (mostly studied by transport methods). Our experimental result is consistent with and supports the previous discussion. In conjunction with the earlier report[10] smaller e-ph coupling for RBM in larger diameter CNTs, previous discussion for LO phonon suggests that a larger diameter CNT tends to have a smaller e-ph coupling, and thus it tends to have a smaller resistance in transport measurements.

The tunable Raman measurements not only can be used for e-ph coupling measurements but also can be very helpful in understanding the physical origin of a Raman feature. We study the Raman feature around 1700 cm^{-1} and assign it as a combination mode of a low energy (about 400 cm^{-1}) phonon and a high energy (about 1300 cm^{-1}) phonon, both at k-space zone boundary. Our assignment is based not only on the 1700 cm^{-1} Raman feature's shape and energy connections to other modes but also on the connection in phonon dispersions of the three modes.

The Raman features above 1700 cm^{-1} are generally believed to be two-phonon scattering modes, either second harmonic or combination modes of one-phonon scatterings, because the *G* band has the highest energy modes for one phonon scatterings in CNTs. In 2000 it was proposed that the Raman features from 1700 cm^{-1} to 1800 cm^{-1} were the combination modes of RBM and *G* modes.[14] The study was performed on a large ensemble of CNTs, and the Raman spectra were the envelopes of different modes from different CNTs. A later study with CVD grown CNTs reassigned the Raman features to be the second harmonic of the infrared-active oTO mode at 867 cm^{-1} in graphite and named this mode the *M* mode, after the appearance of the mode showed double peaks resembling as "M" in the report.[13] Here we propose that the *M* mode is intrinsically just one peak, the *M* mode should be the combination of two zone-boundary phonons, whose energies are about 400 cm^{-1} and 1300 cm^{-1}.

We have three reasons to contradict the assignment, the 1700 cm^{-1} feature as the overtone of the oTO band. First an explanation, the *M* mode is just one peak, is more straightforward and consistent with the large amount of experimental data from different groups. We measured high energy modes for about 10 CNTs. Seven of them show noticeable *M*-mode signals. CNT (9,4) and CNT (9,7)'s *M*-mode spectra are in Fig. 1. The other three CNTs' spectra are plotted in Fig. 3(a). Another two CNTs' spectra are reported in a separate paper.[27] All of those seven CNTs show only a single peak feature for the *M* mode. (CNT3 could be multiple CNTs, giving the complex structure of the *G* band. Even so, the *M* mode is still a single peak in this case.) Zhang *et al.* measured 54 CNTs.[28] Fifty of them show only one peak, and another four show double peaks. Zhang *et al.* attribute the doubling to the ensemble samples. The second reason is that the energy of the *M* mode doesn't match the twice energy of the oTO modes. Both the oTO band and *M* mode are measured simultaneously for CNT1. Sample spectra of the *M* mode and oTO band under 1.562-eV excitation are shown in Fig. 3(a) and 3(b). The excitation was scanned from 1.49 eV to 1.59 eV. The features and locations of the *M* mode and oTO band are consistent as the excitation-energy changes. The oTO band consists of a main peak at 894 cm^{-1} ($q = 0$ mode) and a broad feature starting at 837 cm^{-1} ($q = 2k$ mode). The *M* mode has energy of 1734 cm^{-1}. Half energy of
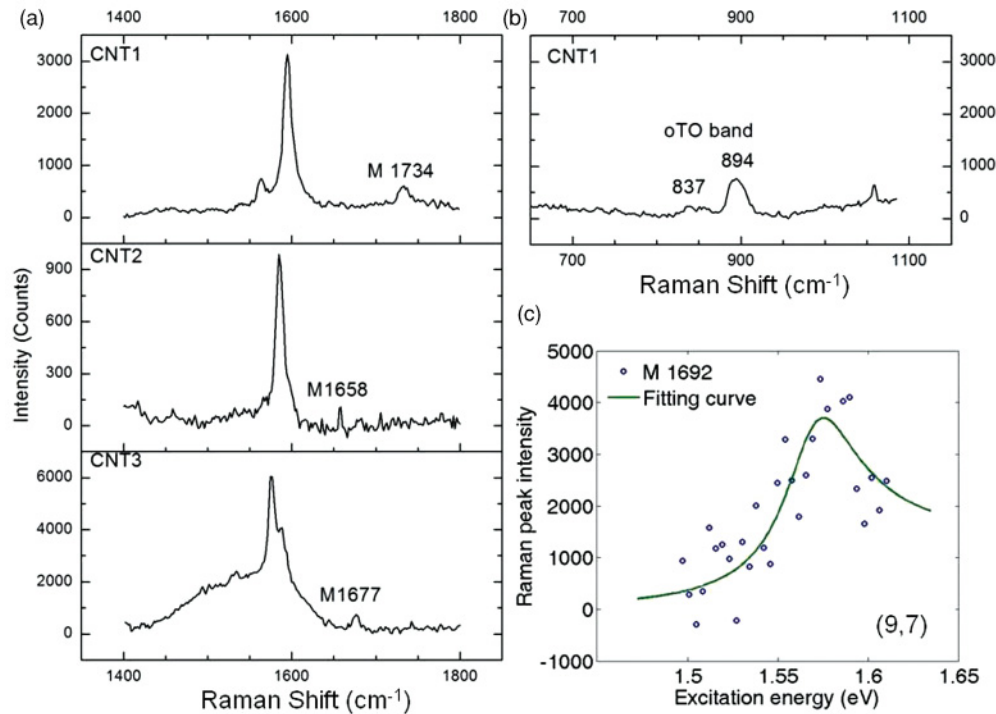
FIG. 3. (Color online) (a) *M*-mode spectra of three other CNTs: CNT1 is under 1.562-eV excitation, CNT2 is under 1.535-eV excitation, and CNT3 is under 1.595-eV excitation; (b) oTO-band spectrum of CNT1 under 1.562-eV excitation; (c) Raman-excitation profile and fitting of the *M* mode of CNT (9,7), the hollow circles are experiment data and the curve is fitting result. Raman intensities are in arbitrary units.

the *M* mode is 867 cm^{-1}, where the middle dip is in oTO band and oTO-phonon density of states vanishes. The third reason is that the *M* mode's Raman excitation profile doesn't match the shape of an overtone of a Γ-point phonon. The *M*-mode Raman excitation profiles of CNT (9,4) and CNT (9,7) are shown in Fig. 2(f) and Fig. 3(c). The data in Fig. 2(f) is fitted for two different situations, one for a combination mode (the green solid curve), and another for an overtone of a Γ-point phonon (the red dash curve). For a combination mode of two zone-boundary phonons, the RRSE profile should be the same as one Γ-point phonon with the combined energy, because the resonance at the intermediate state is forbidden because of the momentum conservation. Therefore, Eq. (1) applies to combination modes of two zone-boundary phonons as well, with E_{ph} representing the total phonon energy. The green solid curve in Fig. 2(f) is the fitting result from (1), which composes only two resonances at E_{ii} and $E_{ii}+1709$ cm^{-1}. If the overtone formula—Eq. (2)—is used for the fitting, as the red dash line, a big mismatch will happen between data and fitting at the high energy side. A similar situation happens to the (9,7) *M*-mode RRSE data as well. This mismatch is attributable to the third, intermediate resonance at $E_{ii}+\omega_M/2$ in the overtone formula,[10] conflicting with the fact that the experiment data does not have such a resonance. Another paper presents the *M*-mode excitation profiles with much larger tunable ranges and also does not show such intermediate resonance at $E_{ii}+\omega_M/2$.[27]

We propose that the Raman feature at 1700 cm^{-1} is the combination mode of two zone-boundary phonons (about 400 cm^{-1} and 1300 cm^{-1}). First, our experimental data show a very good matching in the mode energies. In Fig. 1(b) of

CNT (9,7) the sum of the energy of mode 403 and mode 1288 is 1691 cm^{-1}, which is identical (within experiment errors) to the *M* mode (1692 cm^{-1}). Mode 403 possibly derives from the LA mode in graphite, at the first (lowest) zone-boundary modes area (around 400 cm^{-1}) in CNTs after zone folding.[15,16] The mode 1288 shows a dispersion, -45 cm^{-1}/eV (see Fig. 4) is certainly a double resonance phonon feature. Both the mode 403 and mode 1288 are likely zone boundary-phonon modes and show up with finite defects in CNTs. The (9,4) CNT's Raman spectra do not show this low energy zone-boundary mode and the high-energy mode, which both are defect dependent. At same time, we studied the phonon dispersions of the three modes as a function of the laser-excitation energy for CNT (9,7) and the mode 1709 of CNT (9,4). The results are plotted in Fig. 4. All the spectra data are automatically processed by a MATLAB program using a Lorentz line-shape fitting. No human preference is involved other than removing of the edge-excitation spectra when the Raman feature signal is below noise level. Individual spectra data show a few cm^{-1} fluctuations in phonon energies because we can't determine the laser excitation energy accurately to below 1 cm^{-1} level, and the subtraction of a linear background might introduce additional errors. However, the statistics of all the data still give us an insight into the phonon dispersions of the modes. In Fig. 4 the phonon-dispersion data are plotted as black squares; the experimental data are fitted with a linear function, and fitting results are plotted as red lines as well. For CNT (9,7) the mode 403 shows a dispersion of 22 ± 7 cm^{-1}/eV, the mode 1288 shows a dispersion of -45 ± 15 cm^{-1}/eV, and the mode 1692 shows a dispersion of -20 ± 18 cm^{-1}/eV. For CNT (9,4) the mode 1709 shows a dispersion
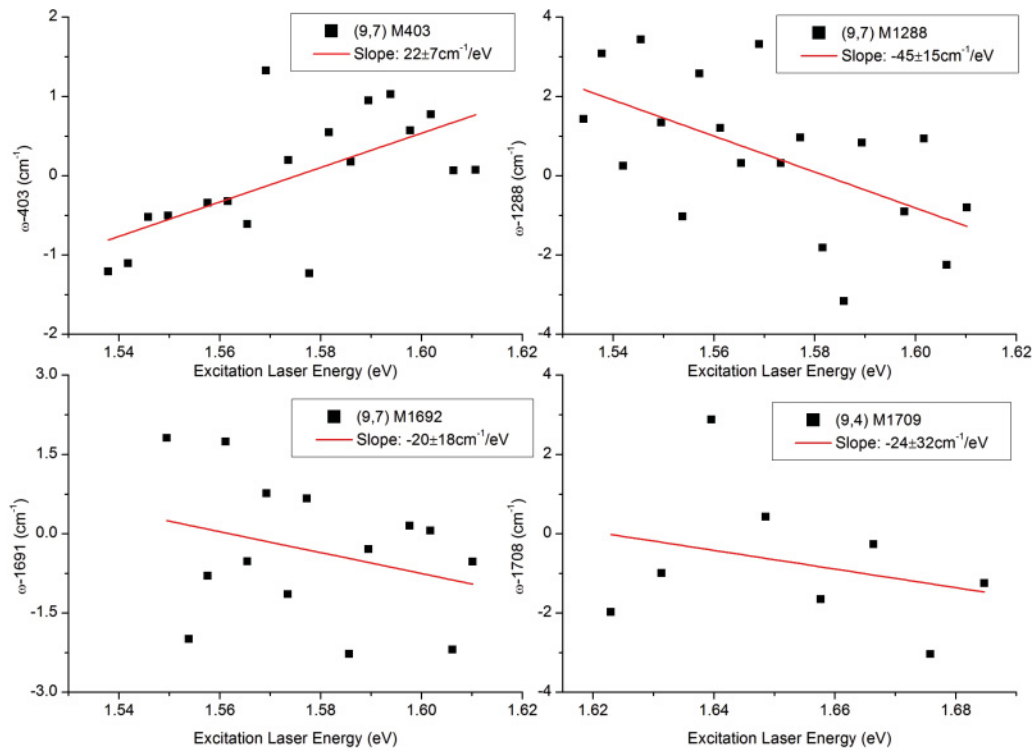
FIG. 4. (Color online) Phonon-dispersion data of CNT (9,7) M403 (upper left), M1288 (upper right), M1692 (lower left), and CNT (9,4) M1709 (lower right). The black squares are the experimental data; the red lines are the linear fitting results. The slopes of the fittings are listed in the legends.

of -24 ± 32 cm^{-1}/eV. For CNT (9,7) the dispersion of M1692 is closely matching the sum of dispersions of M403 and M1288. This strongly supports that the M1692 is the combination mode of M403 and M1288. Meanwhile, the dispersion of M1692 in (9,7) and M1709 in (9,4) are consistent with the previously reported -26 cm^{-1}/eV dispersion of the "*M*-" mode.[15] The M1288 in CNT (9,7) shows -45 ± 15 cm^{-1}/eV dispersion and is opposite of previously reported dispersion of *D* mode in metallic CNTs.[29,30] According to reported calculation only metallic CNTs should show *D* mode.[30] Is the M1288 the *D* mode of CNT (9,7)? Does *D*-mode dispersion vary largely for CNTs with different chiralities? For now we leave these questions open in this report. Overall, we believe that our experimental results together with previous reports on the "*M*" mode are in conflict with the assumption of the overtone of the oTO mode. A combination mode of two zone-boundary phonons ($\sim$400 cm^{-1} and $\sim$1300 cm^{-1}) is a better explanation for the $\sim$1700 cm^{-1} feature. We also propose to name this $\sim$1700 cm^{-1} feature as *C* mode, because this is a combination mode and the physical origins of its subcomponent modes are still uncertain.

In summary we experimentally measured the e-ph coupling matrix elements of different phonon modes, RBM and *G* for (9,4) and (9,7) CNTs. Our experimental results for Γ-point

RBM, G^- (iTO) and G^+ (LO) modes are in good agreement with theoretical calculations from tight-binding model with deformation potential physical picture. The e-ph coupling for G^+ modes in the two CNTs are about 30 meV or 12.5 eV/Å, which links very well with the value for transport measurements. We further discussed the diameter and chirality dependence, and found that the e-ph coupling for G^+ mode tends to be smaller for larger diameter CNTs. The coupling strengths for the G^+ mode should range from 23 to 83 meV for 1-nm-diameter CNTs, and 12 to 58 meV for 2-nm-diameter CNTs. In comparison the e-ph coupling of the G^+ mode is an order of magnitude stronger than those of other measured phonon modes, including the RBM mode. The previous information is very helpful in understanding the e-ph scattering phenomena in optical or electron transport measurements. We also discussed the physical origin of a Raman feature around $\sim$1700 cm^{-1}, based on both phonon energies and phonon dispersions and assigned it as the combination mode of two zone-boundary phonons, which have energies of $\sim$400 cm^{-1} and $\sim$1300 cm^{-1}.

*yan.yin@aphy.iphy.ac.cn
†goldberg@bu.edu
[1] J. Y. Park, S. Rosenblatt, Y. Yaish, V. Sazonova, H. Ustunel, S. Braig, T. A. Arias, P. W. Brouwer, and P. L. McEuen, Nano Lett. **4**, 517 (2004).

[2] A. Zazunov, D. Feinberg, and T. Martin, Phys. Rev. Lett. **97**, 196801 (2006).
[3] T. Tsuneta, L. Lechner, and P. J. Hakonen, Phys. Rev. Lett. **98**, 087002 (2007).
[4] Z. Yao, C. L. Kane, and C. Dekker, Phys. Rev. Lett. **84**, 2941 (2000).

[5] D. F. Santavicca, J. D. Chudow, D. E. Prober, M. S. Purewal, and P. Kim, Nano Lett. (to be published).

[6] V. Perebeinos, J. Tersoff, and P. Avouris, Phys. Rev. Lett. **94**, 086802 (2005).

[7] A. W. Bushmaker, V. V. Deshpande, M. W. Bockrath, and S. B. Cronin, Nano Lett. **7**, 3618 (2007).

[8] M. Lazzeri, S. Piscanec, F. Mauri, A. C. Ferrari, and J. Robertson, Phys. Rev. B **73**, 155426 (2006).

[9] L. Luer, C. Gadermaier, J. Crochet, T. Hertel, D. Brida, and G. Lanzani, Phys. Rev. Lett. **102**, 127401 (2009).

[10] Y. Yin, A. N. Vamivakas, A. G. Walsh, S. B. Cronin, M. S. Ünlü, B. B. Goldberg, and A. K. Swan, Phys. Rev. Lett. **98**, 037404 (2007).

[11] A. P. Shreve, E. H. Haroz, S. M. Bachilo, R. B. Weisman, S. Tretiak, S. Kilina, and S. K. Doorn, Phys. Rev. Lett. **98**, 037405 (2007).

[12] J. Yan, Y. B. Zhang, P. Kim, and A. Pinczuk, Phys. Rev. Lett. **98**, 166802 (2007).

[13] V. W. Brar, Ge. G. Samsonidze, M. S. Dresselhaus, G. Dresselhaus, R. Saito, A. K. Swan, M. S. Ünlü, B. B. Goldberg, A. G. Souza Filho, and A. Jorio, Phys. Rev. B **66**, 155418 (2002).

[14] S. D. M. Brown, P. Corio, A. Marucci, M. A. Pimenta, M. S. Dresselhaus, and G. Dresselhaus, Phys. Rev. B **61**, 7734 (2000).

[15] M. S. Dresselhaus, G. Dresselhaus, R. Saito, and A. Jorio, Phys. Rep. **409**, 47 (2005).

[16] V. N. Popov, V. E. Van Doren, and M. Balkanski, Phys. Rev. B **61**, 3078 (2000).

[17] Y. Homma, Y. Kobayashi, T. Ogino, and T. Yamashita, Appl. Phys. Lett. **81**, 2261 (2002).

[18] Y. Yin, A. G. Walsh, A. N. Vamivakas, S. B. Cronin, A. Stolyarov, M. Tinkham, W. Bacsa, M. S. Ünlü, B. B. Goldberg, and A. K. Swan, IEEE J. Sel. Top. Quantum Electron. **12**, 1083 (2006).

[19] A. Jorio, M. A. Pimenta, A. G. Souza, R. Saito, G. Dresselhaus, and M. S. Dresselhaus, New J. Phys. **5**, 139.1 (2003).

[20] R. M. Martin and L. M. Falicov, *Light Scattering in Solids I, Chapter 3* (Springer, New York, 1975), pp. 79–101.

[21] M. Canonico, G. B. Adams, C. Poweleit, J. Menendez, J. B. Page, G. Harris, H. P. van der Meulen, J. M. Calleja, and J. Rubio, Phys. Rev. B **65**, 201402 (2002).

[22] Y. Yin, Ph.D. Dissertation, Boston University, 2006.

[23] A. N. Vamivakas, Y. Yin, A. G. Walsh, M. S. Ünlü, B. B. Goldberg, and A. K. Swan, e-print arXiv:cond-mat/0609197v1 (2006).

[24] J. Jiang, R. Saito, G. G. Samsonidze, S. G. Chou, A. Jorio, G. Dresselhaus, and M. S. Dresselhaus, Phys. Rev. B **72**, 235408 (2005).

[25] M. Machon, S. Reich, and C. Thomsen, Phys. Rev. B **74**, 205423 (2006).

[26] J. Jiang, R. Saito, A. Gruneis, S. G. Chou, G. G. Samsonidze, A. Jorio, G. Dresselhaus, and M. S. Dresselhaus, Phys. Rev. B **71**, 205420 (2005).

[27] A. G. Walsh, A. N. Vamivakas, Y. Yin, S. B. Cronin, M. S. Ünlü, B. B. Goldberg, and A. K. Swan, Nano Lett. **7**, 1485 (2007).

[28] L. Zhang, L. M. Huang, M. Lind, V. Liao, S. O'Brien, and Z. H. Yu, J. Phys. Chem. C **113**, 16432 (2009).

[29] J. Maultzsch, S. Reich, U. Schlecht, and C. Thomsen, Phys. Rev. Lett. **91**, 087402 (2003).

[30] J. Maultzsch, S. Reich, and C. Thomsen, Phys. Rev. B **64**, 121407 (2001).